Turkish Journal of Computer and Mathematics Education Vol.12 No.7 (2021), 1051-1061
Research Article

Mechanical Properties And Microstructure Characterization Of Friction Stir Welded Joint Of Dissimilar Aluminum Alloy AA2024 And AA7050

A. Nait Salah*[1], M. Kaddami[2], Husain Mehdi[3]

[1,2]Laboratory "Physical Chemistry of Processes and Materials" Faculty of Science and Technology, Hassan First University of Settat, Morocco
[3]Department of mechanical engineering, Meerut institute of technology, Meerut, India

Article History: Received: 11 January 2021; Revised: 12 February 2021; Accepted: 27 March 2021; Published online: 16 April 2021

Abstract: The friction stir welding (FSW) have a wide range of applications in manufacturing industries, aerospace engineering, shipbuilding, and automobile industries. The dissimilar aluminum alloys AA2024 and AA7075 with thickness of 3 mm have been successfully fabricated by FSW with different tool rotational speed (TRS) (1000 to 1800 rpm) with a constant feed rate of 85 mm/min with the tilt angle of 0°. The FSWed joint was characterized by mechanical properties and microstructural at room temperature and it was observed that all the welded joints produced a sound welded joint with a smooth surface except 1800 rpm. The maximum tensile strength (214.79 MPa), and micro-hardness (118) at the nugget zone was observed at tool rotation 1200 rpm and 1000 rpm respectively with constant traverse speed 85 mm/min and tilt angle 0°. The effect of tool rotation on FSW welded joint also improve the ductility of the welded joints at a certain limit, FSW welded joint with tool rotation 1200 rpm was more ductile than the other FSW welded joint due to fine grain structure. The grains size in the nugget zone at higher tool rotation (1200 rpm) was observed much finer (7.9 µm) than the other rotational speed. The minimum residual stress of 14 MPa was observed at TRS of 1200 rpm, whereas maximum residual stress of 98 MPa was observed at 1800 rpm.

Keywords: Friction stir welding, Microstructure, Tensile strength, Micro-hardness

1. Introduction

The demand for lightweight materials like aluminum alloys AA6061, AA7050, and AA2024, etc. with high strength is continuously increasing in the aerospace and automobile industries. These Al-alloys are more prevalent in automobiles, aircraft, and other engineering application due to low thermal expansion, high resistance to wear, and high thermal conductivity [1-2]. The ultimate tensile strength and proof strength of FSWed joint of AA6061 with matrix composite reinforced with Al_2O_3 led to a decrease of 28% and 43% respectively as compared to parent metal [3]. The FSW/FSP was developed by TWI in 1991[4], which was a relatively novel welding technique that has revealed its great potential in joining of similar or dissimilar aluminum alloys.

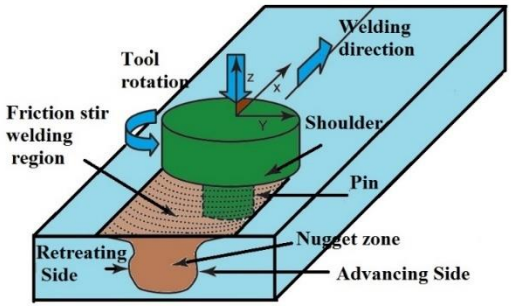

Figure 1: Schematic diagram of friction stir welding

A non-consumable rotating tool is used during friction stir welding process which is plunged into the base plate under the axial load. Due to frictional heat generation between the rotating tool and the base plate, the material around the rotating tool probe is softened and reveal plastically deformed from the front to the back and joining takes place. This entire joining process was accomplished in a solid state as shown in fig. 1 [5].The influence of processing parameters on TIG+FSP joint of AA6061 and AA7075 using RSM with central composite design (CCD) method and observed the maximum joint efficiency and tensile strength of 95% and 60.8% and 255 MPa at TRS of

1300 rpm with TS of 45 mm/min [6]. The Taguchi and RSM technique to analyze the optimized value of ultimate tensile stress of FSWed joint of AA2024 and found that the maximum joint efficiency of 84% and tensile strength 386 MPa at TRS of 750 rpm, shoulder diameter of 12 mm with a feed rate of 10 mm/min [7]. Currently, a new hybrid welding technique is used to reduce the fusion welding defect such as micro-crack, porosity, and large grain structure by FSP on TIG welded joint and observed the excellent microstructure and mechanical properties of dissimilar aluminum alloys of AA 6061 and AA7075 [8, 9], the computational fluid dynamics the model also developed to predict the material flow and temperature distribution of the hybrid welding technique by fluent [10-13]. In FSW of Al-alloys, a significant change has occurred in mechanical properties and microstructure in different areas that might be easily achieved by severe thermal cycles and strain rates [14, 15]. The material and the tool design play a significant role during the joining process. The FSP/FSW can modify the material properties in terms of tribological performance, joint strength, ductility and modification of microstructure, reduce casting defect, and enhanced wear resistance [16-18]. The tool rotational speed ranges from 500-700 rpm did not have a significant effect of abrasive wear characteristic and tensile strength of Mg/SiC nanocomposite, whereas tool traverse speed (TS) ranges from 30-60 mm/min observed a momentous effect on both wear resistance characteristic and tensile strength of Mg/SiC nanocomposite [19]. The variation of coefficient of friction and sliding distance was observed higher in composite reinforced MoS2 as compare to Zn, whereas composite reinforced MoS2 revealed higher wear resistance as compared to base material Al-17Si and zinc composite [20]. The tool rotational speed has a dominating parameter to enhance the wear resistance of the FSP sample of AS-castA356, when the TRS increases, wear resistance increasing [21]. At low TRS, the hardness of the welded joint of AA5754 increases and observed wear rate of 80 mg with tunnel defect. An augmented of wear resistance may be recognized to the combined effect of solid solution, and grain boundary strengthening mechanisms [22]. Therefore, the above-mentioned works only yielded limited and preliminary investigation of the mechanical properties and microstructure of welded joint of aluminum alloys. In this work the effect of tool rotational speed was observed to enhance the mechanical properties and microstructure of dissimilar aluminum alloys of AA7050 and AA2024.

2. Materials and Methods

A CNC (computer numerical control) milling machine was used for the FSW process. The dimensions of the base metal were taken as 120 mm x 40 mm x 3 mm. A non-consumable tool of square cross-section made of tool steel (H13) was used as shown in fig. 2. The tool rotational speed has been taken ranges from 1000 to 1800 rpm, while the feed rate and tilt angle kept constant 85 mm/min and 0°. The chemical composition and mechanical properties of base metal AA2024 and AA7050 as shown in Tables 1 and 2. The welded cross-section was polished with different grades (400-2000) of emery papers and analyzed microstructure by scanning electron microscope (SEM model ZEISS EVO 18 special edition).

Figure 2: Cross section of friction stir welding tool

The tensile test was carried out by a UTM (universal testing machine) at room temperature as per ASTM E8 standard as shown in fig. 3. For each welded plate, three specimens were tested and the average of these three results were taken. For residual stress observation at the stir zone of the FSWed joint of AA2024 and AA7050, the cosα

method was used for determining the residual stress with the help of the Pulstec μ-X360 apparatus. The incident angle of the X-ray was set as 35° and the time was used during this process 8-10 min. The images of the residual stress profile of the welded samples were captured at 50μm resolution with approximately beam spot size was 3.2 mm for 1.4 mm pinhole collimator.

Table1: Chemical composition of parent materials

Material	Si	Cu	Fe	Zn	Mg	Mn	Cr	Ti	Al
AA2024	0.4	4.2	0.6	0.2	1.4	0.5	0.15	0.15	Bal.
AA7050	0.2	2.5	0.12	5.8	1.8	0.1	0.03	0.05	Bal.

Table 2: Mechanical properties of base material

Material	Yield Strength (MPa)	Tensile strength (MPa)	Hardness (HV)
AA2024	132.04	295.24	95
AA7050	186.84	389.65	129

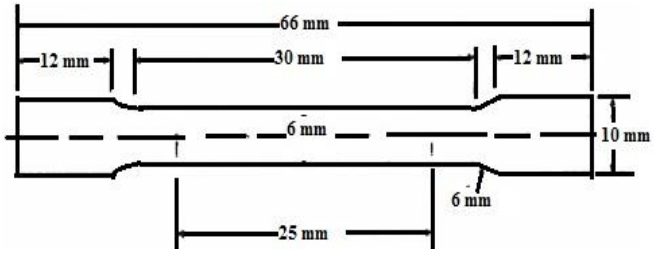

Figure 3: Tensile sub test specimen as per ASTM E8

3. Results and Discussions

3.1 Characterization of Microstructure

3.1.1 Different zones of the FSW

The parent material in the stir zone (SZ) was exposed to heat and severe deformation. The highest temperature during FSW observed in the SZ. The maximum temperature in the SZ is dependent on the process parameters [18-19]. Because of high temperature and deformation, the dynamic recrystallization (DRX) has occurred in the SZ which created the fine grain size and modifies the microstructure, due to this, an onion ring structure was seen in SZ shown in fig. 4. The stable phases were occurred because of the cooling rate, which also prevents the addition of unstable phases.

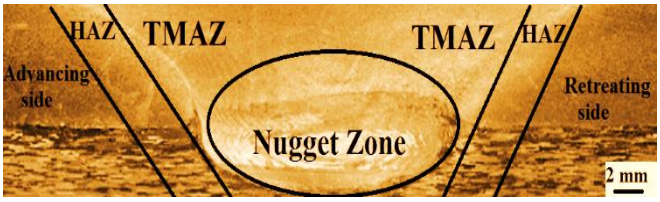

Figure 4: Different zone of the friction stir welded joint

The thermo mechanically affected zone (TMAZ) experiences the heat and plastic deformation. In this zone, the elongated and highly deformed structure was observed. The recrystallization does not occur in TMAZ due to a lack of plastic strain. The temperature of the heat-affected zone (HAZ) was lower than the TMAZ region but has a significant effect if the microstructure is thermally unstable. The plastic deformation does not occur in HAZ. The

grain structure was similar to base material up to a temperature of 250°, when the temperature is above 250° will have an important effect on the microstructure of sediments [20].

3.1.2 Effect of process parameters on microstructure of welded joint

The microstructures of the welded joint at the weld stir zone at different TRS (1000, 1200, 1400, 1600, and 1800 rpm) were shown in fig. 4. It can be seen that the weld zone was invariable showed fine and equiaxed grains structure at all TRS due to high temperature and severe plastic deformation which was adequate to caused dynamic recrystallization (DRX) by traverse and rotational speed throughout the FSW.

Due to frictional heat input and severe plastic deformation in the FSWed joint, the original coarse microstructure was breaking up and observed newly equiaxed grains in the weld nugget zone (WNZ). This has resulted in many microstructural modifications included micro-texture transformation, DXZ, and coarse precipitation. The effect of TRS on the microstructure of the weld nugget zone in the friction stir welded joint of AA2024 and AA7050 as shown in fig.5. The temperatures at the weld nugget zone for dissimilar aluminum alloy reached 400-480°C. The temperature in the weld nugget zone was higher than the adjacent region (i.e. HAZ and TMAZ). The extensive plastic deformation and the frictional heat generate fine and equiaxed grains in the WNZ [21]. The dynamic recrystallization of the nugget zone resulted in the formation of fine and equiaxed grains structure in the WNZ. The fine-grain size was observed when the tool rotational speed increases from 1000 rpm to 1200 rpm. The grain size in the nugget zone at tool rotational speed of 1200 rpm was finer than that of tool rotational speed of 1000, 1400, 1600, and 1800 rpm. The average grain size in the WNZ was observed at 7.9 µm at 1200 rpm, whereas 20.4 µm grain size was observed at 1800 rpm as shown in fig.5. This may be attributed to the lower temperature in the retreating side [22].

The WNZ was characterized by equiaxed and fine grains structure because of dynamic recrystallization (DRX) on in divergence to the base metal microstructure. The DRX occurs in the WNZ due to high thermal exposure and strain during the FSP. The degree of heat input and material deformation are both decreased when the TRS increased at constant traverse speed [23].

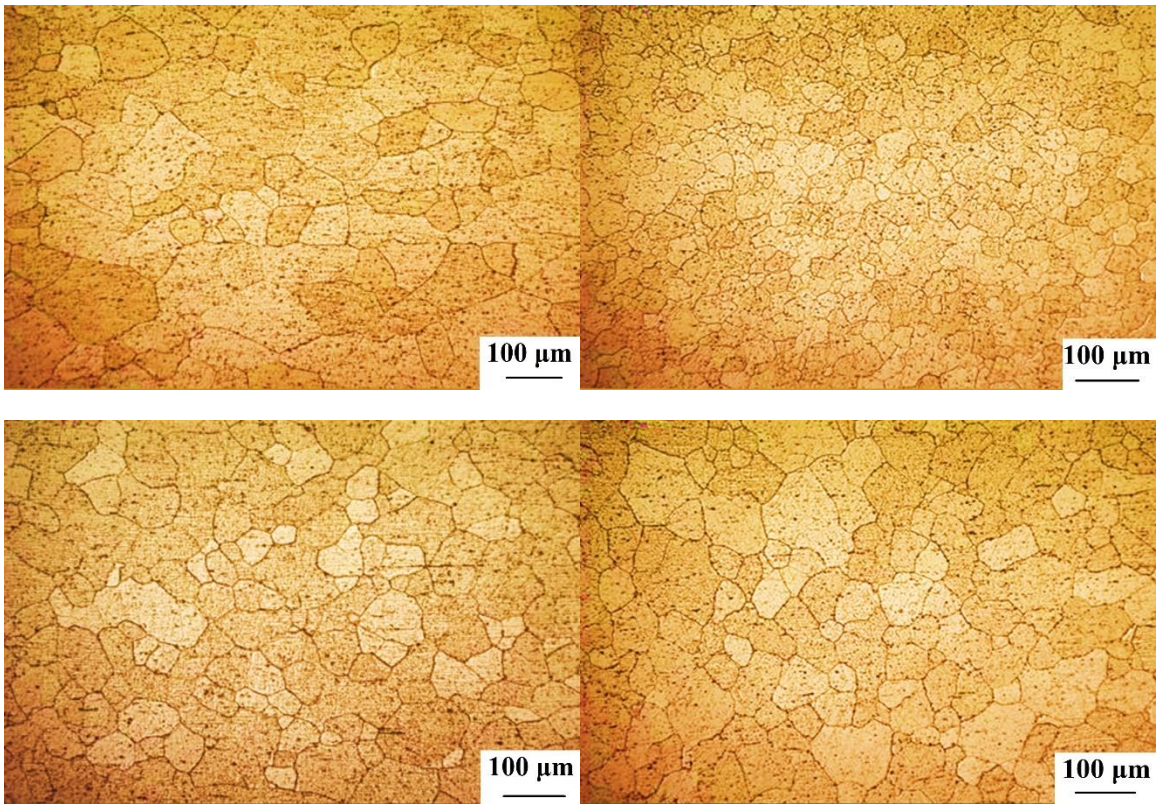

Figure 4: Microstructure of weld stir zone, (a) 1000 rpm, (b) 1200 rpm, (c) 1400 rpm, (d) 1600 rpm, (e) 1800 rpm

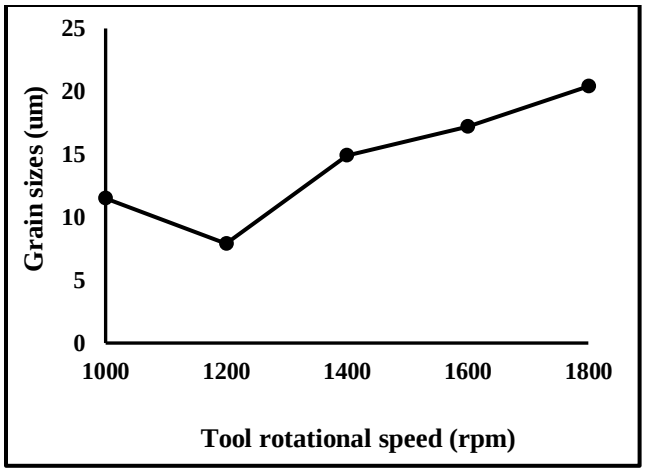

Figure 5: Variation of grain sizes to the tool rotational speed

3.2 Tensile strength

The effect of tool rotational speed on tensile strength of FSWed joint of dissimilar Al-alloys of AA7050 and AA2024 was observed. The tensile specimens were fractured in HAZ and thermo-mechanically affected zone (TMAZ) where the hardness was located as a minimum. In other dissimilar aluminum alloys, the FSW joints were failed at the location of the HAZ [24]. The tensile stress of FSWed joints was lower than the parent material. The tensile stress of the FSWed joints has a tendency to increase with the precipitation hardening of the parent metal. The strength and ductility of defect-free welded joints are dependent on the thermal properties of base metal [25-26]. The coarse grains precipitates within the grains boundary was observed due to dissolution of the fine precipitates during FSW process which influence the tensile properties of the weldments. The percentage elongation and ductility of the weldment were lower than those of the parent material [27]. If the welded joints are free from defects, then the tensile strength of the weldments is only dependent on the hardness of the FSW joints [28]. The stress-strain curve of the FSWed joints with various TRS as shown in fig. 6. It can be seen that the highTRS produced higher tensile strength. The tensile strength of FSWed joints increases as TRS increases. The maximum tensile strength of 214.79 MPa was observed at tool rotational speed of 1200 rpm, whereas the minimum tensile strength of 166.38 MPa was observed at tool rotational speed of 1800 rpm. It was concluded that the tensile properties of the FSWed joints are highly affected by TRS [29].

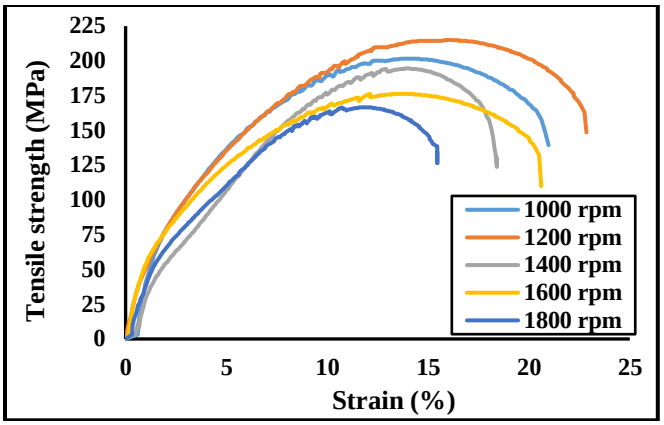

Figure 6: Stress strain diagram of friction stir welded joint of AA2024 and AA7050 at different tool rotational speed

As the TRS increased, the tensile strength also increased. At lower TRS, the heat was generated at the WNZ which inadequate to strain the plasticized metal that occurred in inferior consolidation of the metal which deteriorated the mechanical properties of the FSWed joints.

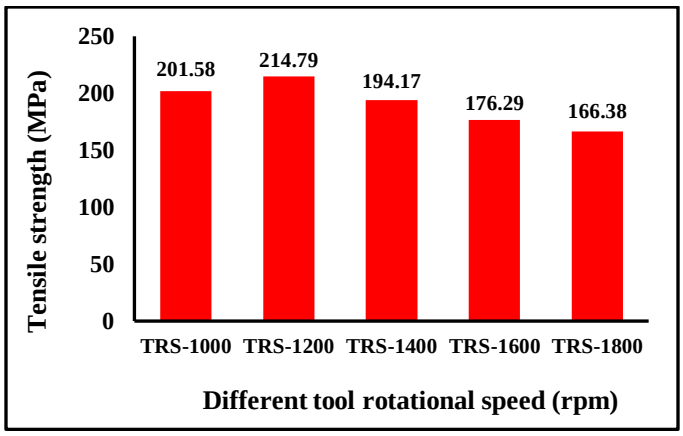

Figure 7: Variation of tensile strength and tool rotational speed

3.1 Micro-hardness analysis

In order to analyzed the micro-hardness at various zone, the hardness values were measured in the transverse direction of the FSwed joint. Fig. 8 illustrate the influence of TRS on the micro-hardness of the different zones. The hardness test was performed at seven different places namely parent metal-1 (AA 2024), A.S, HAZ, TMAZ, WNZ, and parent metal-2. At each place, three different reading was taken, and mean values opted. The hardness in NZ was slightly higher as compared to TMAZ and heat affected zone which was attributed to small grain size. The decreasing trend of micro-hardness in TMAZ is due to the dissolution of precipitates and lower hardness was pronounced in the HAZ due to the coarsening of precipitates [30]. The slightly low hardness was observed in HAZ due to the coarsening of strengthening precipitates and desertion of the Guinier-Preston (G.P) zones. More probably comprehensive severe coarsening and dissolution of precipitates occurred in TMAZ due to the analogous effect of solution treatment. The material experienced higher temperatures in the nugget zone due to re-precipitation after complete dissolution takes place. When the AA7050 was positioned on the A.S and low TRS was used then the transition of micro-hardness in the WNZ from aluminum alloy 7050 to AA2024 was more gradual and observed more effective material mixing. Fig. 8 demonstrates the variation of micro-hardness from HAZ to TMAZ the FSWed joints of AA7050 and AA2024 at different values of TRS. From the figure, it was seen that the hardness value at the WNZ increases when the tool rotational speed increased. Moreover, the increase of tool rotational speed caused the increment of hardness due to fine microstructure and low heat concentration [31]. The microhardness directly affects the phase dispersion microstructure and dislocation density. In the conventional friction stir welding process, inducing high heat input and thermal cycle cause grain growth and roughen the microstructure of the WNZ.

The processing parameters of FSP have a more dominating factor over the hardness value because the hardness values are less significant in affecting the mechanical properties of the weldment [10]. The microhardness variation plays a significant role to detect the metallurgical phase in the welded region. Due to the cooling rate and solidification sequence, the micro-hardness and grain size were detecting the major effect at the bottom and middle of the welded joint. In fig.8, it is shown that by increasing the TRS, the hardness at the nugget zone increases and reaches to a maximum value at their intermediate level. The maximum hardness (110 HV) was found at TRS of 1200 rpm, whereas minimum hardness (90 HV) was obtained at TRS of 800 rpm.

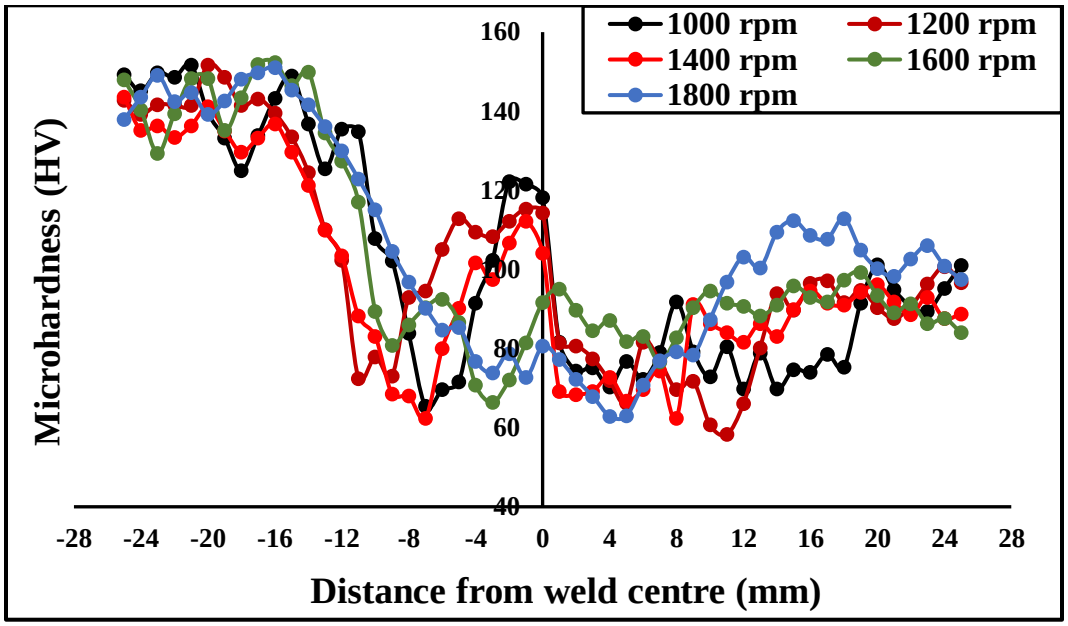

Figure 8: Distribution of micro-hardness of FSW welded joint of AA 2024 and AA 7050 with different rotational speed

Table 3: Mechanical properties of welded joint of AA2024 and AA7050 at different tool rotational speed

Tool rotational speed (rpm)	Traverse speed (mm/min)	Tilt angle (°)	Tensile strength (MPa)	Hardness at stir zone (HV)	Residual stress at stir zone (MPa)	Grain size (μm)
TRS-1000	85	0	201.58	118	38	11.5
TRS-1200	85	0	214.79	114	14	7.9
TRS-1400	85	0	194.17	104	67	14.9
TRS-1600	85	0	176.29	92	74	17.2
TRS-1800	85	0	166.38	81	98	20.4

3.3 Residual stress analysis [12]

The residual stresses were measured of polished welded specimens by Pulstec μ-X360 apparatus with the help of cosα method, the residual stress could affect both positive and negative effect on the welded specimens. The compressive residual stress plays a positive effect on the welded specimens whereas tensile residual stress may lead to a negative effect on the FSWed joints. Fig. 9 shows the residual stress profile measured on the bottom and top of the weldment of the SZ. These residual stress profiles were used for measuring the residual stress measurements by the cosα method. The equations for the measurement of residual stress by the cosα method are as follows.

$$q_s = \begin{bmatrix} \cos\eta \sin\psi_0 + \sin\eta \cos\psi_0 \cos\alpha \\ \cos\eta \sin\psi_0 \sin\phi_0 + \sin\eta \cos\psi_0 \sin\phi_0 \cos\alpha + \sin\eta \cos\phi_0 \sin\alpha \\ \cos\eta \cos\psi_0 + \sin\eta \sin\psi_0 \cos\alpha \end{bmatrix}$$

The strain projection along (η, α) coordinates can be writtenas in terms of scattering vector and strain component as

$\varepsilon_\alpha = q_i q_j \varepsilon_{ij}$

$$\varepsilon_{ij} = \frac{1+\nu}{E}\sigma_{ij} - \delta_{ij}\frac{\nu}{E}\sigma_{kk} \qquad (1)$$

So, the strain projection may be written as

$$\varepsilon_\alpha = \frac{1+\nu}{E} q_i q_j \sigma_{ij} - \frac{\nu}{E} \sigma_{kk} \quad (2)$$

Now, defining two parameters a_1 and a_2 for linear determination of σ_{11} and σ_{22}

$$a_1 = \frac{1}{2}[(\varepsilon_\alpha - \varepsilon_{\pi+\alpha}) + (\varepsilon_{-\alpha} - \varepsilon_{\pi-\alpha})] \quad (3)$$

$$a_2 = \frac{1}{2}[(\varepsilon_\alpha - \varepsilon_{\pi+\alpha}) - (\varepsilon_{-\alpha} - \varepsilon_{\pi-\alpha})] \quad (4)$$

After re-expressing of equations (26) and (27) to lead the final relationship for this method.

$$a_1 = \frac{1+\nu}{E} \sin 2\psi_0 \sin 2\eta \cos\alpha [\sigma_{11}(1+\cos 2\phi_0) + \sigma_{22}(1-\cos 2\phi_0) + 2\sigma_{12}(\sin 2\phi_0)] \quad (5)$$

$$a_2 = \frac{1+\nu}{E} \sin\psi_0 \sin 2\eta \sin\alpha [\sigma_{22} \sin 2\phi_0 - \sigma_{11} \sin 2\phi_0 + 2\sigma_{12} \cos 2\phi_0)] \quad (6)$$

at $\phi_0 = 0$, the above equations will be

$$a_1 = \sigma_{11} \frac{1+\nu}{E} \sin 2\psi_0 \sin 2\eta \cos\alpha \quad (7)$$

$$a_2 = 2\sigma_{12} \frac{1+\nu}{E} \sin\psi_0 \sin 2\eta \sin\alpha \quad (8)$$

Thus the term cosα in the equation (30) was the origin of the name for this method

The value of stresses after re-expression maybe written as

$$\sigma_{11} = -\frac{E}{1+\nu} \frac{1}{\sin 2\psi_0 \sin 2\eta} \quad (9)$$

$$\sigma_{12} = -\frac{E}{2(1+\nu)} \frac{1}{\sin 2\psi_0 \sin^2 \eta} \quad (10)$$

The residual stresses will affect the fractured strength, buckling strength, and fatigue strength, and it also affected by lifetime prediction of the weldment. The residual stress distribution profile was observed from the weld center. the tensile stresses commence to appear longitudinally as the weld metal cools down, while the compressive stresses produced by the expanding hot material lead to plastic straining due to the low compressive yield strength. The magnitude of the transverse residual stresses may be below the yield strength of the welded joint [32]. The transverse residual stresses were notably smaller in WNZ when the TRS of FSW was increased. The negative residual stresses were observed in the area of HAZ, which specified that the tensile residual stresses should exist near the start and endpoints of the FSWed joint. The residual stresses gradually increase towards the end of the FSWed weld line. The residual stress at the stir zone decreases when the TRS increases, the maximum compressive residual stress (98 MPa) in the stir zone was observed at a rotational speed of 1800 MPa, whereas minimum tensile residual stress (14 MPa) was observed at a tool rotational speed of 1200 rpm. The residual stress profile peaks for all welded specimens were lies between 145 to 180°. The blue contour indicates a minimum amount of residual stress, while the red contour indicates a higher concentration of residual stress at SZ of the weldment as shown in fig.9.

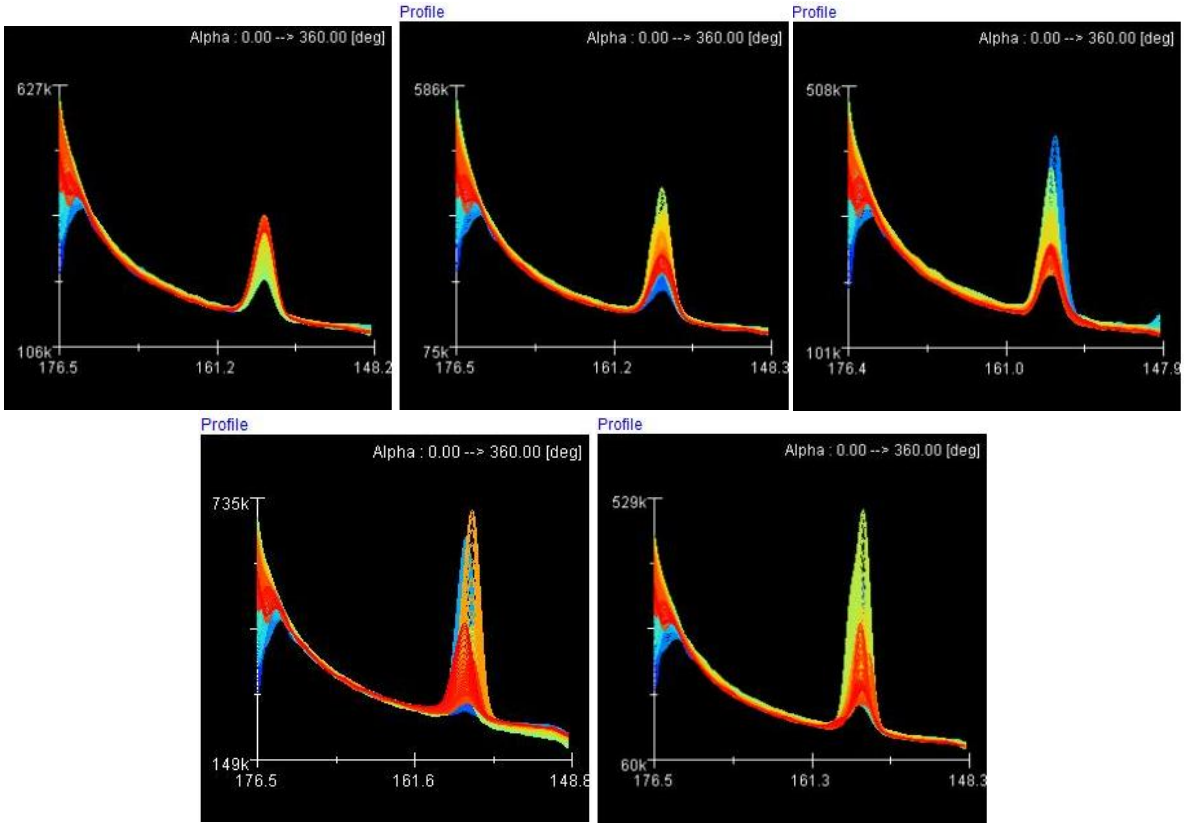

Figure 9: Residual stress profile at the stir zone of the welded joint, (a) 1000 rpm, (b) 1200 rpm, (c) 1400 rpm, (d) 1600 rpm, (e) 1800 rpm

4. Conclusions

The analysis of friction stir welding on dissimilar aluminum alloys of AA2024 and AA7050 have been successfully fabricated. The mechanical characterization of FSW welded joints were investigated using experimental methodology by adjusting tool rotational speeds. The following conclusions have been made from the experimental work.

- The maximum tensile strength (214.79 MPa), and micro-hardness (118) at nugget zone was observed at tool rotation 1200 rpm and 1000 rpm respectively with constant traverse speed 85 mm/min and tilt angle 0°.
- The effect of tool rotation on FSW welded joint also improve the ductility of the welded joints at certain limit, FSW welded joint with tool rotation 1200 rpm were more ductile than the other FSW welded joint due to fine grain structure.
- Beyond the tool rotational speed of 1200 rpm, the ductility and tensile strength gradually decreases due to turbulence of softened material at higher tool rotational speed in which intermetallic compound and second phase particles were clustered to be segregated ones and coarse and non-homogeneous distribution in the aluminum matrix.
- The grains size in the nugget zone at higher tool rotation (1200 rpm) was observed much finer (7.9 µm) than the other rotational speed.
- The minimum residual stress of 14 MPa was observed at tool rotational speed of 1200 rpm, whereas maximum residual stress of 98 MPa was observed at 1800 rpm.

References

1. J.F. Guo, H.C. Chen, C.N. Sun, G. Bi, Z. Sun, J. Wei, Friction stir welding of dissimilar materials between AA6061 and AA7075 Al alloys effects of process parameters, Materials and Design 56 (2014) 185–192.

2. S. Madhavarao , Ravi Varma Penmetsa , G S V Seshu Kumar , Ch Ramabhadri Raju, K.Tarun Kumar, Investigation On Mechanical Properties Of Friction Stir Welded AA7075 & AA6061 Joints, Materials Today: Proceedings 18 (2019) 2288–2297.
3. Thomas WM, Nicholas ED, Needham JC, Murch MG, Templesmith P, Dawes CJ. Friction-stir butt welding. G.B. Patent 9125978.8, UK: 1991.
4. R.S. Mishra, Z.Y.Ma, Friction stir welding and processing, Materials Science and Engineering: R: Reports, 50(1), 1-78, 2005.
5. L. Ceschini, I. Boromei, G. Minak, A. Morri, Microstructure, tensile and fatigue properties of AA6061/20 vol.%Al_2O_{3p} friction stir welded joints, Composites: Part A 38 (2007) 1200–1210.
6. Husain Mehdi & R.S. Mishra (2020) An experimental analysis and optimization of process parameters of AA6061 and AA7075 welded joint by TIG+FSP welding using RSM, Advances in Materials and Processing Technologies, DOI: 10.1080/2374068X.2020.1829952
7. K. Boulahem, S. Ben Salem, and J. Bessrour (2018), "Prediction model of ultimate tensile strength and investigation on microstructural characterization of friction stir 1 welded AA2024-T3," Int. J. Adv. Manuf. Technol., vol. 95, no. 1–4, pp. 1473–1486.
8. Husain Mehdi, R.S Mishra, Effect of Friction Stir Processing on Microstructure and Mechanical Properties of TIG Welded Joint of AA6061 and AA7075. Metallogr. Microstruct. Anal. 9, 403–418 (2020). https://doi.org/10.1007/s13632-020-00640-7.
9. Husain Mehdi, R.S. Mishra. Study of the influence of friction stir processing on tungsten inert gas welding of different aluminum alloy. SN Appl Sci 2019; 1: 712
10. Husain Mehdi, R.S. Mishra, Influence of Friction Stir Processing on Weld Temperature Distribution and Mechanical Properties of TIG-Welded Joint of AA6061 and AA7075. Trans Indian Inst Met 73, 1773–1788 (2020). https://doi.org/10.1007/s12666-020-01994-w.
11. Husain Mehdi, R.S. Mishra, Effect of friction stir processing on mechanical properties and heat transfer of TIG welded joint of AA6061 and AA7075, Defense Technology (2020), https://doi.org/10.1016/j.dt.2020.04.014.
12. Husain Mehdi, R.S. Mishra, Investigation of mechanical properties and heat transfer of welded joint of AA6061 and AA7075 using TIG+FSP welding approach, Journal of Advanced Joining Processes Volume 1, 2020, https://doi.org/10.1016/j.jajp.2020.100003.
13. Husain Mehdi, R.S. Mishra (2019), Analysis of Material Flow and Heat Transfer in Reverse Dual Rotation Friction Stir Welding: A Review, International Journal of Steel Structure,vol-19, issue2, pp 422-434.
14. Abolusoro, Olatunji P., and Esther T. Akinlabi. "Wear and corrosion behaviour of friction stir welded aluminium alloys—an overview." *Int J Mech Prod Eng Res Dev* 9.3 (2019): 967-982.
15. Sutton M, Reynolds A, Wang DQ, Hubbard C. A study of residual stresses and microstructure in 2024-T3 aluminum friction stir butt welds. J Eng Mater Technol Trans ASME 2002;124(2):215–21.
16. Sato Y, Park SHC, Kokawa H. Microstructural factors governing hardness in friction-stir welds of solid-solution-hardened Al alloys. Metall Mater Trans A 2001;32(12):3033–42.
17. Alidokht SA, Abdollah-zadeh A, Soleymani S, Saeid T, Assadi H (2012) Evaluation of microstructure and wear behaviour of friction stir processed cast aluminum alloy. Mater Charact 63:90– 97.
18. Santella ML, Engstrom T, Storjohann D, Pan TY (2005) Effects of friction stir processing on mechanical properties of thecast aluminum alloys A319 and A356. Scripta Materialia 53:201– 206
19. Leon, J. Stephen, and V. Jayakumar. "An investigation of analytical modelling of friction stir welding." *Int. J. Mech. Prod. Eng. Res. Dev* 9.1 (2019).
20. Rao AG, Rao BRK, Deshmukh VP, Shah AK, Kashyap BP (2009) Microstructure refinement of a cast hypereutectic Al–30Si alloy by friction stir processing. Mater Lett 63:2628–2630.
21. M. Deepan, Chandan Pandey, N. Saini, M. M. Mahapatra, R. S. Mulik, Estimation of strength and wear properties of Mg/SiC nanocomposite fabricated through FSP route, Journal of the Brazilian Society of Mechanical Sciences and Engineering, 39, 4613–4622 (2017).
22. N. Saini, C. Pandey, S. Thapliyal, D. K. Dwivedi, Mechanical Properties and Wear Behavior of Zn and MoS Reinforced Surface Composite Al- Si Alloys Using Friction Stir Processing, Silicon, 10, 1979–1990 (2018).
23. Sima Ahmad Alidokht, Amir Abdollah-zadeh, Soheil Soleymani , Tohid Saeid, Hamid Assadi, Evaluation of microstructure and wear behavior of friction stir processed cast aluminum alloy, Materials Characterization 63 (2012) 90– 97
24. El-Shennawy, M., Adel A. Omar, and M. Ayad. "Similar and Dissimilar Friction Stir Welding of AA7075." *International Journal of Mechanical Engineering (IJME)* 3.4 (2014): 69-86.

25. Sebastian Balos, Danka Labus Zlatanovic, Petar Janjatovic, Miroslav Dramicanin, Dragan Rajnovic, Leposava Sidjanin, Wear Resistance Increase by Friction Stir Processing for Partial Magnesium Replacement in Aluminium Alloys, IOP Conf. Series: Materials Science and Engineering 329 (2018) 012017.
26. Devireddy, K. R. I. S. H. N. A. J. A., et al. "Analysis of the influence of friction stir processing on gas tungsten arc welding of 2024 aluminum alloy weld zone." *Int. J. Mech. Prod. Eng. Res. Dev* 8.1 (2018): 243-252.
27. Humphreys F, Hatherly M. Recrystallization and related annealing phenomena. 2nd ed. New York: Pregamon; 2004.
28. Koilraj M, Sundareswaran V, Vijayan S, Rao SRK. Friction stir welding of dissimilar aluminum alloys AA2219 to AA5083 – Optimization of process parameters using Taguchi technique. Mater Des 2012;42:1–7.
29. Midling OT, Oosterkamp LD, Bersaas J. Friction stir welding aluminium process and applications. In: Proceedings of the seventh international conference on joints in aluminium, INALCO98; 1998.
30. Backlund J, Norlin A, Andersson A. Friction stir welding-weld properties and manufacturing techniques. In: Proceedings of the seventh international conference on joints in aluminium, INALCO98; 1998.
31. Resan, Kadhim K., et al. "Influence of Temperature on Fatigue Life for Friction Stir Welding of Aluminum Alloy Materials." *International Journal of Mechanical & Mechatronics Engineering IJMME-IJENS* 18.02 (2018).
32. Hakan Aydın, Ali Bayram, Agah Uguz, Kemal Sertan Akay, Tensile properties of friction stir welded joints of 2024 aluminum alloys in different heat-treated-state, Materials and Design 30 (2009) 2211–2221.
33. Hirata T, Oguri T, Hagino H, Tanaka T, Chung SW, Takigawa Y, et al. Influence of friction stir welding parameters on grain size and formability in 5083 aluminum alloy. Mater Sci Eng, A 2007; A456 (1–2):344–9
34. Simar A, Brechet Y, Meester B, de Denquin A, Gallais C, Pardoen T. Integrated modeling of friction stir welding of 6xxx series Al alloys: process, microstructure and properties. Progr Mater Sci 2012;57:95–183.
35. Resan, Kadhim K., et al. "Influence of Temperature on Fatigue Life for Friction Stir Welding of Aluminum Alloy Materials." *International Journal of Mechanical & Mechatronics Engineering IJMME-IJENS* 18.02 (2018).
36. Azimzadegan T, Serajzadeh S. An Investigation into microstructures and mechanical properties of AA7075-T6 during friction stir welding at relatively high rotational speeds [J]. Journal of Materials Engineering Performance, 2010, 19(9): 1256−1263.
37. Sevvel, P. and Jaiganesh,V.: A detailed investigation on the role of different Tool Geometry in Friction Stir Welding of various Metals & their Alloys, Proceedings of the International Colloquium on Materials, Manufacturing & Metrology – ICMMM, August 8- 9, pp 103 – 107, 2014.
38. Altenkirch, A. Steuwer, P. J. Withers, S. W. Williams, M. Poad, S. W. Wen. Residual stress engineering in friction stir welds by roller tensioning. Science and Technology of Welding and Joining, 14(2): 85-192.